2021

Mass Measurement, Visualization and Signal Pattern Based Calibration of Capacitive Sensors for Measuring Void Fraction in Headers

Hongliang Qian
University of Illinois at Urbana and Champaign, hqian7@illinois.edu

Pega Hrnjak
University of Illinois at Urbana and Champaign

Mass Measurement, Visualization and Signal Pattern Based Calibration of Capacitive Sensors for Measuring Void Fraction in Headers

Hongliang QIAN[1], Pega HRNJAK[1, 2*]

[1]Air Conditioning and Refrigeration Center, the University of Illinois at Urbana-Champaign, 1206 West Green Street, Urbana, IL 61801, USA

[2]Creative Thermal Solutions, 2209 Willow Rd., Urbana, IL, USA

* Corresponding Author: pega@illinois.edu +1-217-390-5278

ABSTRACT

This paper presents the calibration procedures of the capacitive sensors for measuring void fraction in headers with R134a. The sensors utilize the difference of dielectric constants between the liquid and vapor phases of the two-phase mixture. The 3D printed header has eleven microchannel-tube protrusions. Eleven capacitive sensors are located between protrusions. All sensors are made to be identical as much as possible in the manual fabrication procedures. Because the electric field within each sensor is not perfectly uniform, sensors need to be calibrated before measuring void fraction. Another transparent 3D printed header with the same inner geometry is installed at the same location of the facility for visualization and pressure drop measurement purposes. By controlling valves, the flow is directed to either header. The calibration is based on three methods: mass measurement (quick-closing valves, QCV), visualization (with a high-speed camera), and capacitive signals obtained from eleven individual sensors. After the calibration procedure, all sensors are ready to measure the void fraction in vertical headers.

1. INTRODUCTION

Microchannel heat exchangers (MCHEs) are widely encountered in air-conditioning systems. With the compact geometry, the refrigerant charge in the MCHE is reduced from conventional finned tube heat exchangers. However, the prediction models of charge in the headers with refrigerant are not reported in the literature, to our best knowledge. The void fraction and flow regimes are the two essential parameters that are closely related to the refrigerant charge. Due to the complexity of the header geometry and flow patterns within the header, a systematic way to measure void fractions in headers with refrigerant is also missing in the literature. Some common methods used to measure void fractions in experiments are X-ray/γ-ray absorption (Isbin *et al.*, 1957), optical (Wojtan *et al.*, 2005), wire mesh probe (Da Silva *et al.*, 2010), quick-closing valves (QCV) (Qian & Hrnjak, 2019) and capacitive method (Abouelwafa & Kendall, 1980; Canière *et al.*, 2007; Qian & Hrnjak, 2020). Compared to other methods, capacitive sensors are non-intrusive. The cost of the sensor is relatively low.

Eleven capacitive sensors are designed and built to measure void fractions in headers simultaneously based on the same principles from the former study (Qian & Hrnjak, 2020, 2021). This method utilizes the difference of permittivity between the liquid and vapor phases of two-phase flow. However, the electric field within the sensors is not uniform. The sensors are hand-made and not fully identical. A calibration procedure is necessary before the sensors can be applied to measure void fraction in headers. In this paper, the calibration procedures for both vertical and horizontal headers are proposed. After the calibration, sensors are capable of measuring void fractions in the vertical headers between every two protrusions.

2. Experimental method

The schematic drawing of the facility is shown in Figure 1. Pure subcooled liquid refrigerant (R134a) is pumped through a mass flow meter with a gear pump. Enthalpy is obtained from refrigerant pressure ($P_{sub,i}$) and temperature ($T_{sub,i}$) before the heater. The flow is then heated by an electric heater, which is control by a VFD. The power of the heater is measured by a watt transducer before the VFD. With the measured power, mass flow rate, and inlet enthalpy, refrigerant quality after the heater is determined. After the refrigerant is mixed in the mixer, it flows into the test section, which includes two parts: *visualization/DP measurement part* and *capacitive signal/average void fractions part* (Figure 2). The model of pressure transducers is Sensotec's TJE, and the differential pressure sensor is Rosemount. T-type thermocouples are used to measure temperature. All the pressure transducers, differential pressure transducer, and thermocouples are calibrated before being applied in the facility, and the uncertainties are listed in Table 1. Both tested parts have the same inner geometry. They are installed at the same height in the facility with the same upstream inlet tubes (500 mm of 9.25mm PFA tube). By controlling valves, refrigerant can pass through either part. Flow regimes are assumed to be identical in both parts for a specific test condition. After refrigerant passes the test section, the refrigerant flows into two coolers whose secondary liquid is glycol then subcooled into liquid condition. The subcooled liquid is fed into the gear pump to finish the loop.

Figure 2 shows the details of both tested parts. For the visualization/DP measurement part (Figure 2a), it is a 3D printed, transparent tube with header-like protrusions. It contains ten protrusions and ten pressure measurement ports. Each protrusion with a thickness of 3 mm has six microchannels. The pitch between two protrusions is 15.8 mm, which is the same as the inner tube diameter without protrusions (D). The other end of each protrusion, which is sealed with a flange, for now, has a socket. It can be easily connected to an aluminum microchannel tube for the following studies. The total length of this test section is 173.8 mm. Both ends of the section are connected to a steel structure and valves. A high-speed camera is used to capture flow regimes with a resolution of 512x512 and a speed of 2200 frames per second (fps). Phantom CV 2.8 from Vision Research Inc. is used to process the video. Pressure measurement ports are named 1 to 10 from low to high. To measure the pressure difference, port number 10 (assumed to be the lowest pressure port) is chosen to be the pressure baseline (connected to the lower-pressure input of the DP sensor). All other nine ports are connected to the higher-pressure input of the DP sensor by switching in a ball-valve system. By this method, the instrumental uncertainties from using multiple DP sensors can be reduced. All clear tubes connecting the DP sensor and the tested parts are heated, and no liquid is observed in the tubes. For the capacitive signals and the average void fraction measurement part (Figure 2b), 11 sensors are applied between 11 tubes in the header. At both ends of the part, two plug valves are installed as quick-closing valves (QCV) to measure the average void fraction. The void fraction measurement procedure is similar to the previous study in tube conditions (Qian & Hrnjak, 2019). The mass flux calculation is based on the minimum cross-sectional area of the header. For each test condition, capacitive signals, the average void fraction, the pressure drop in the header, and visualization results are obtained. Table 2 lists the experimental conditions that have been tested.

The capacitive signals are read directly from sensors in pF for each test condition. Before each set of experiments is conducted, capacitive signals for two base points are measured: capacitive signals for full vapor phase (C_{Vapor}) and full liquid phase (C_{Liquid}). C_{Liquid} is obtained at 33 ºC. Some researches (dos Reis & Goldstein, 2005) indicated that the effect of temperature on relative permittivity of refrigerant vapor phase could be neglected. Hence, C_{Vapor} is measured at room temperature. After signals of the two base points are determined, the capacitive signals for other test conditions ($C_{measured}$) are measured. Time-averaged C_{Vapor}, C_{Liquid} and $C_{measured}$ are also calculated: $\overline{C_{Vapor}}$, $\overline{C_{Liquid}}$ and $\overline{C_{measured}}$. The time-averaged normalized capacitance $\overline{C_{norm}}$ are defined as follows:

$$\overline{C_{norm}} = \frac{\overline{C_{measured}} - \overline{C_{Vapor}}}{\overline{C_{Liquid}} - \overline{C_{Vapor}}} \quad (1)$$

The denominator shows the entire range of signal difference (quality from 0 to 1 for each mass flux). It is assumed constant for the duration of the one set of experiments. The numerator shows how much larger the measured signal is than the full vapor condition. Hence, the normalized signals are typically from 0 (fully vapor) to 1 (fully liquid).

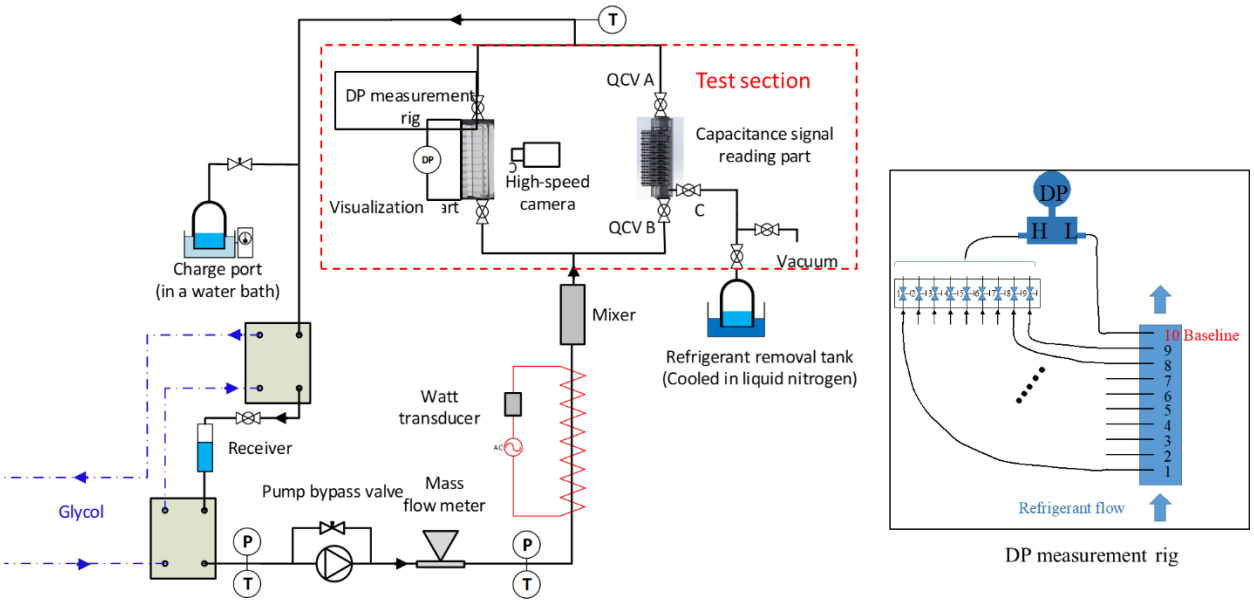

Figure 1: Test facility, test section in the red box, DP measurement rig in the black box

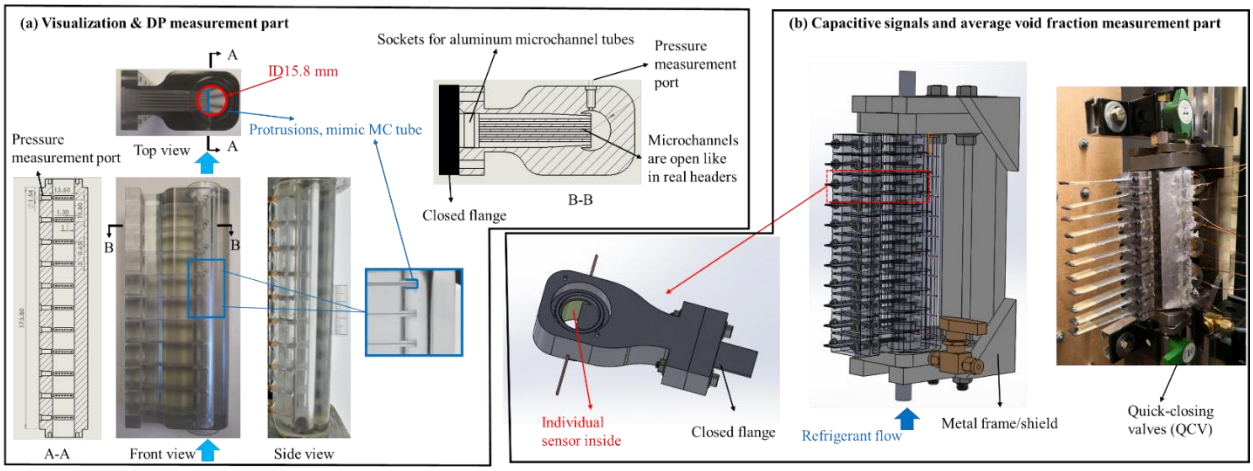

Figure 2: (a) visualization and DP measurement part; (b) capacitive signals and the average void fraction measurement part

Table 1: Instrumental uncertainties

Instrument	Sensotec's pressure transducer	T-type thermocouple	Rosemount 0 to 30 inH_2O DP transmitter	Ohio Semitronics GW5-024CX5 watt transducer
Uncertainty	±1% FS	±0.1 ºC	±0.2% FS	±0.2% FS

Table 2: Test conditions

Working fluid	T_{sat}	Orientation	Mass flux	Vapor quality
R134a	14.5 ºC	Horizontal and vertical upward	28, 43, 58, 72 kg.m-2.s-1	Subcooled liquid, 0.1-0.9 and superheat vapor

3. RESULTS FOR VERTICAL HEADERS

3.1 Visualization

Visualization results are first studied to analyze flow regimes in the test section. In the mass flow rate explored in this paper, we observed three major flow patterns for vertical upward flow: slug flow, churn flow, and annular flow (Figure 3).

Slug flow: Vapor slugs appear periodically with the liquid bridge in the middle. The slugs which are disturbed by protrusions are followed by some small bubbles.

Churn flow: The total effect of shear on interface, pressure gradient, and gravity on a droplet is not constant upwards. Also, due to the disturbance of the protrusions, flow structures are very chaotic.

Semi-Annular flow: Liquid flows along the wall of the tube with vapor in the central core. Some liquid is trapped between protrusions. The interface between liquid and vapor core is wavy.

Flow regimes that appear in this geometry are compared to those in the smooth tubes (Qian & Hrnjak, 2019), and the flow regime map is shown in Figure 4. The visualization indicates that the flow structures of all three flow regimes in the entire test section are similar (Figure 5a). If the flow regime does not change along the section, the local void fraction can be assumed constant and equals to the measured average void fraction by QCV. All eleven sensors can then be calibrated to match the experimentally measured average void fraction. However, it is not enough to support the assumption merely with the 2D visualization results. Pressure drop and capacitive signal results are further analyzed in the following sections.

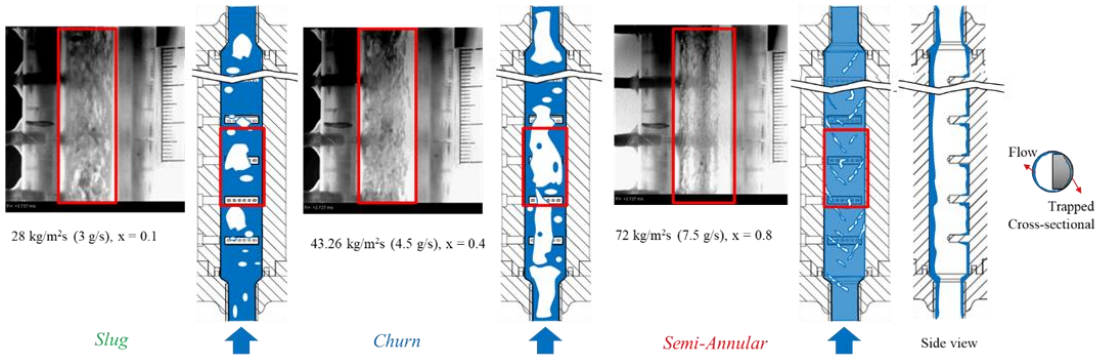

Figure 3: Flow patterns in the tube w/ header-like protrusion (vertical upward flow)

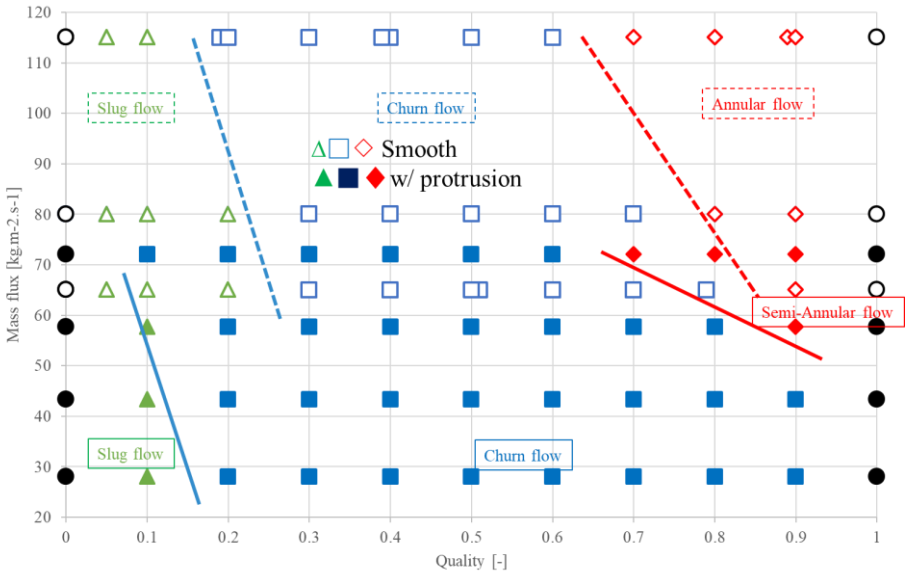

Figure 4: Flow regimes comparison between smooth tube and tube with protrusions

3.2 Pressure drop

Figure 5 shows the control volume of the measured pressure drop. In the control volume, pressure drop can be divided into four major contributions: $\Delta P_{hydrostatic}$, $\Delta P_{friction}$, ΔP_{local} (due to protrusions), and $\Delta P_{expansion/contraction}$. $\Delta P_{hydrostatic}$ is a function of density, ρ. The density ρ within the control volume is also a function of void fractions, α. When the inlet quality is lower, the local void fractions will also be smaller, and the hydrostatic pressure drop is more significant. ΔP_{local} is caused by protrusions. Tuo and Hrnjak (2013) proposed $\Delta P_{local} = k_{loss}\frac{G^2}{2\rho}$, where k_{loss} is the local loss coefficient determined by experiments. ΔP_{local} is again a function of local void fractions. $\Delta P_{friction}$ is a function of many variables, including density, viscosity and surface tension. It is calculated with the model from Friedel (1978). Due to the low mass flow rate, $\Delta P_{friction}$ only accounts for a small portion of the total pressure drop in most cases. $\Delta P_{expansion/contraction}$ is more important at the entrance and the exit of the test section for higher inlet qualities. It is estimated by the model from Chen *et al.* (2010). Overall, the total pressure drop within a control volume is strongly dependent on the local density, which is a function of local void fractions. If the pressure drop along the test section does not change, the local void fractions can be assumed to be constant and equal to the average void fraction measured from QCV. Figure 6 shows the pressure drop results for mass flow rates from 3 to 7.5 g/s. Results show that the pressure drop for all locations are very similar to each other along the section. When the inlet quality is 0 (fully liquid), the measured pressure drop between two protrusions is close to the calculated hydrostatic pressure drop based on the geometry and thermal properties of R134a. In the lower mass flow rate and inlet quality region, which the hydrostatic pressure drop is dominant, as the quality increases, total pressure drop becomes smaller. However, the higher mass flow rate and quality region, the total pressure drop is larger when the inlet quality is higher. In this region, hydrostatic pressure is relatively small, but other contributions ($\Delta P_{friction}$ and ΔP_{local}) are more dominant. When the inlet quality equals to 1 (fully vapor), $\Delta P_{contraction}$ at the exit of the section is relatively larger. It results in a very small or even negative pressure drop at the location of 9-10 (Figure 6).

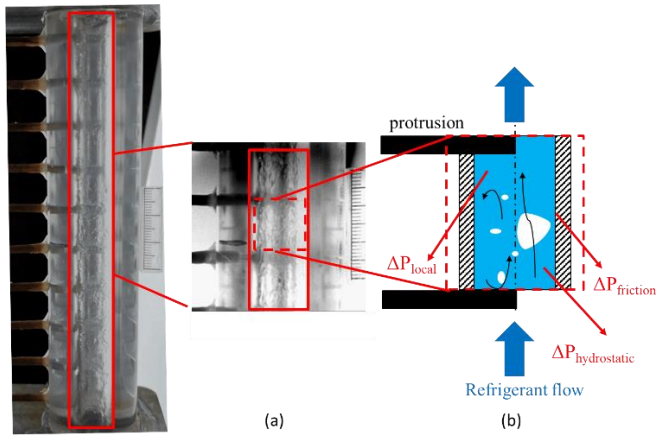

Figure 5: (a) Flow regimes do not change along the section from visualization results; (b) control volume of the measured pressure drop

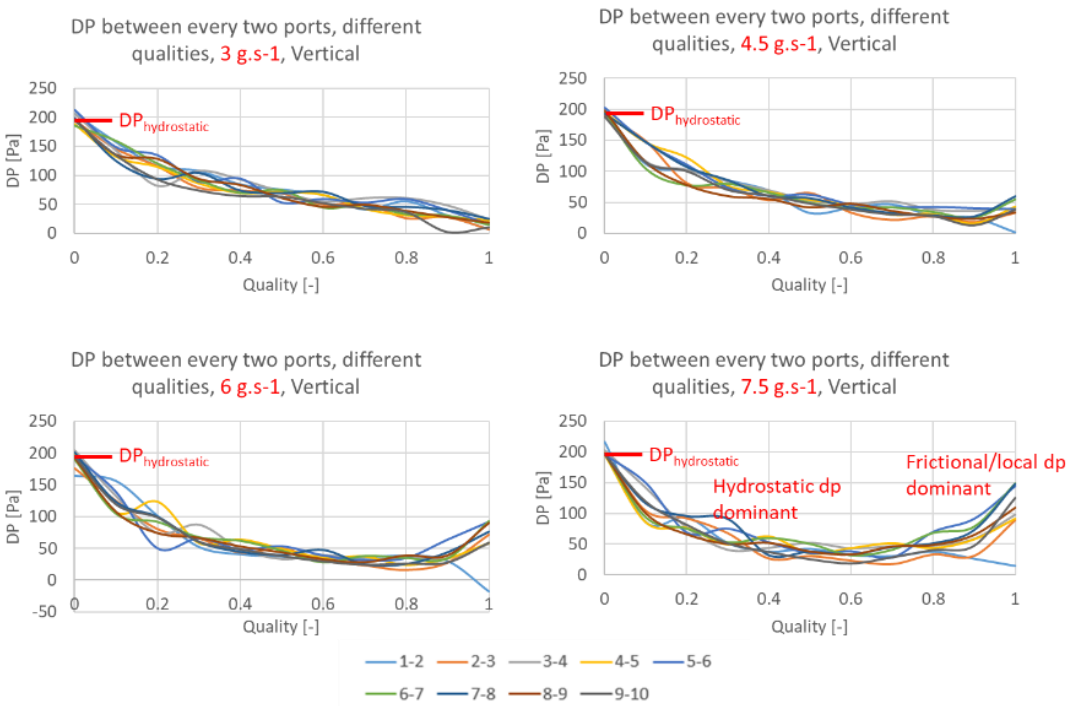

Figure 6: Pressure drop along the section, vertical

3.3 Capacitive signal patterns

Besides the results of the pressure drop along the section, capacitive signals are analyzed to validate the assumption. Drahoš and Čermák (1989) had a review on statistical signal processing for characterizing flow patterns. Three domains can be utilized to characterize flow patterns: *amplitude domain*, *time domain* and *frequency domain*. In the amplitude domain, probability density function (PDF) or probability density estimation (PDE) can be used to estimate signal amplitude distributions. Kernel density estimation (KDE) is a non-parametric method of PDF for using a data set to estimate probabilities. Autocorrelation functions (ACF) and cross-correlation functions (CCF) are usually involved in having statistical analysis in the time domain. For the frequency domain, the signals can be described by the power spectral density (PSD) by using the Fourier transform. It is a function of the frequency and shows at which frequency variations are substantial. In this study, KDE and PSD of the signals and cross-sectional void fractions measured by the sensor are used to characterize flow regimes.

Figure 7 shows the KDE and PSD of the signals from different sensors of vertical upward flow with mass flow rate 7.5 g s^{-1} and inlet quality x_{in}=0.1. Sensors #2, #6, and #9 show a similar shape (one major peak) in the KDE diagram. In the PSD diagram, the dominant frequency from all sensors is between 0-2 Hz. Based on the visualization, pressure drop, and capacitive signals, it is assumed the void fraction along the section does not change and equals the average void fraction measured by QCV.

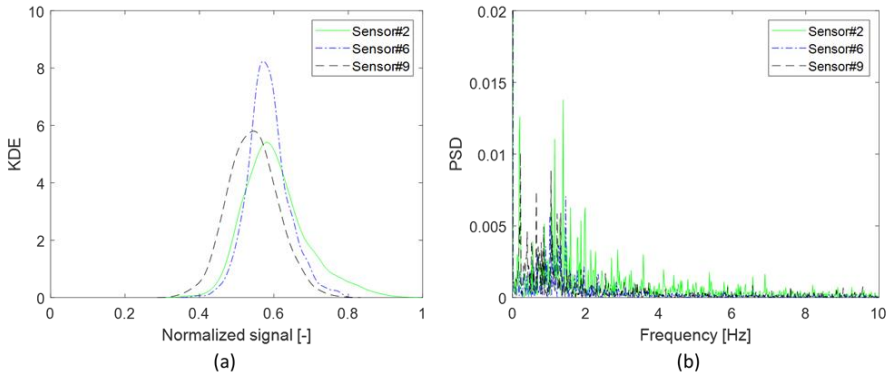

Figure 7: KDE (a) and PSD (b) of the signals from different sensors, vertical upward, 7.5 g s^{-1}, x_{in}=0.1

3.4 Calibration results for vertical headers

Figure 8 shows the sensor calibration results for the vertical upward flow, similar to the calibration procedure of vertical tubes (Qian & Hrnjak, 2020). For each sensor (1 to 11), time-averaged normalized signals are plot with void fractions measured by QCV for all tested conditions. Then with the curve fitting, the relation between capacitive signals and the local void fractions is established. Most void fraction data measured by the sensor falls into the ±10% deviations of the experimental results by QCV for vertical upward flow.

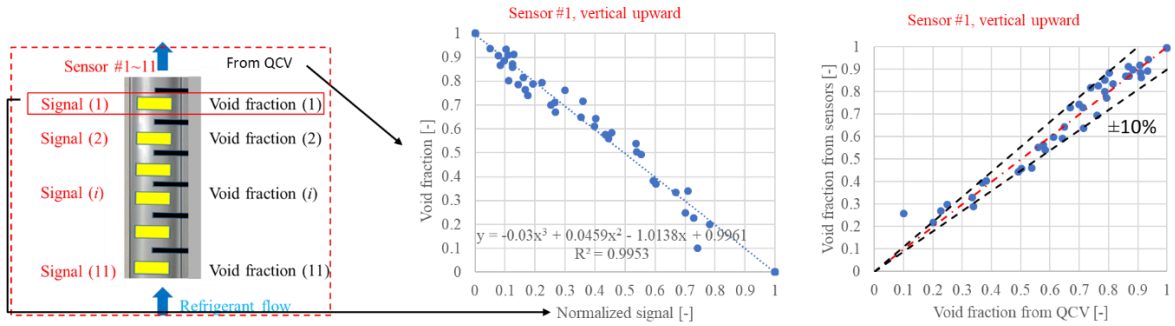

Figure 8: Individual sensor calibration for the void fraction measurement, vertical

4. RESULTS FOR HORIZONTAL HEADERS

The calibration on the configuration of horizontal flow with upward protrusions is conducted first. Visualization results are first obtained with a high-speed camera (Figure 9). Two major flow regimes are observed: stratified-wavy and semi-annular flow. When the inlet quality and mass flux are relatively small, most of the liquid is at the bottom of the header. The boundary between the liquid and vapor phases is wavy. As the quality and mass flux increase, more liquid is entrained with the vapor and carried to the up portion of the header. Some liquid is trapped between protrusions. Hence, it is not a full annular but semi-annular flow.

Flow patterns are changing along the section according to the video footage. Local void fractions (α_i) does not equal to the average void fraction($\bar{\alpha}$, from QCV). This means sensors cannot be calibrated in the way of vertical flow mentioned in the last section. To calibrate each individual sensor, QCV A and B in the test section (from Figure 1) are closed with different liquid refrigerant levels within. After waiting for a period, the liquid is fully stratified. Hence, all local void fraction is equal and can be calculated from the average void fraction from QCV (Figure 10a). Then all 11 sensors are calibrated with different liquid levels, and the relation between void fractions and capacitive signals is found (Figure 10b). Further validation is carried out in the extremely low flow rate condition. In such a condition, the liquid-vapor interface does not touch protrusions (stratified/stratified-wavy flow). Visualization, void fractions from QCV, and signals from calibrated sensors are combined in the validation procedure. The liquid-vapor boundary is captured and digitalized based on an inner tube in the footage (Figure 11). Liquid fraction (1-α) is calculated from the digitalized boundary in the coordination. The liquid fraction from the visualization and sensors agree well (Figure 12a). The liquid fraction from the QCV and sensor are also similar (Figure 12b). The repeatability of the sensors is also tested with relatively good results (Figure 12c).

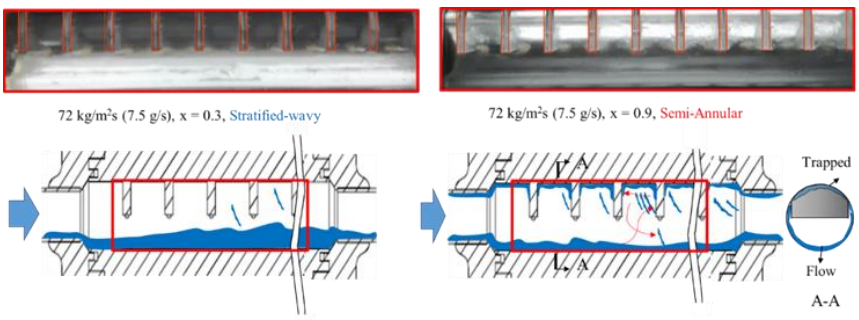

Figure 9: Flow patterns in the tube w/ header-like protrusion (horizontal flow with upward protrusions)

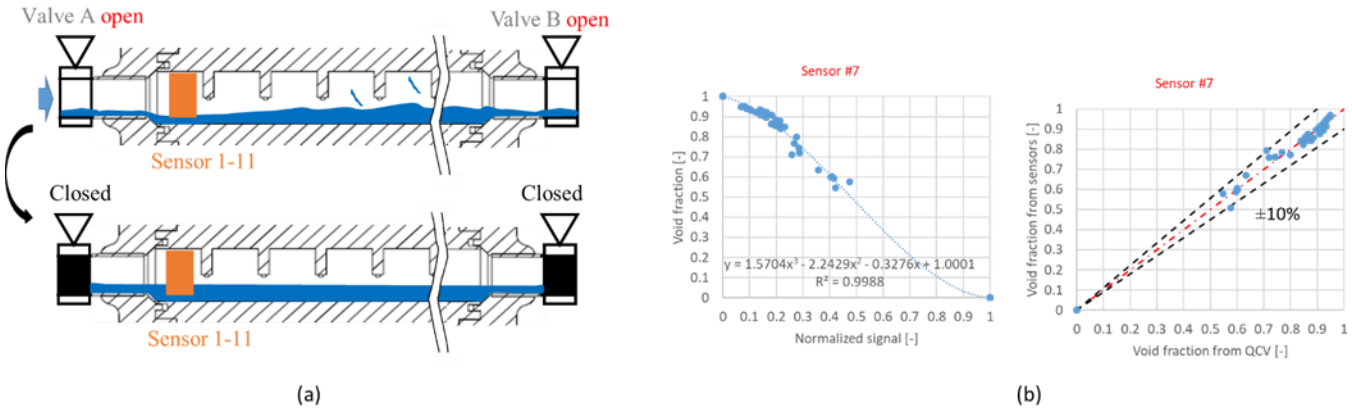

Figure 10: Individual sensor calibration for horizontal flow with upward protrusions, (a) calibration method; (b) calibration results

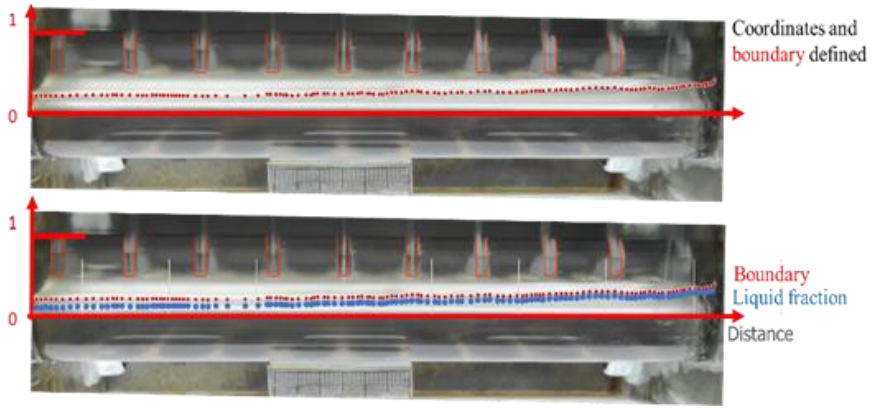

Figure 11: Visualization and coordination building of low-flowrate condition

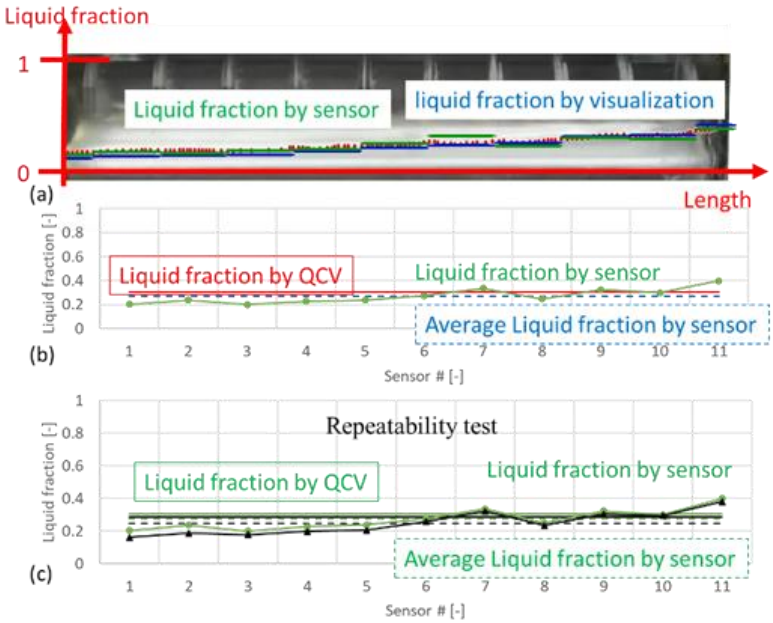

Figure 12: Low-flowrate condition validation

The void fraction in this configuration is always larger than 0.5 due to the upward protrusions. The experiments with downward protrusions are also conducted to finish the whole-range calibration. Figure 13 shows the flow regimes for this configuration. More liquid is trapped between protrusions due to the influence of gravity. When the quality is relatively small, the wavy liquid-vapor boundary is above protrusions. As the quality and mass flux increase, most of the boundary is lower than protrusions. Liquid either passes through the gaps between protrusions and tube wall or is carried by the vapor. The boundary is step-like in the videos.

Sensors are also calibrated in the no-flow condition, similar to the upward protrusion condition. The relations between signals and void fractions are established by changing the liquid level within the sensor. Figure 14 shows the relation between void fractions and normalized signals for both upward and downward protrusion configurations. As shown in the diagrams, the relations from some of the sensors are continuous, which is preferred. This means these sensors are symmetrical, which is not influenced by the orientation of the header. However, some sensors provide discontinuous relations for these two configurations. This may be because that all sensors are not fully identical and symmetric due to the individual-making procedures. If the sensors are fully identical, such as being made by the assembly line, the uncertainties for horizontal header void fraction measurement will be reduced. For now, the sensor will only be used with the upward protrusion configuration. Further calibration or modification may be needed before using it for other horizontal configurations.

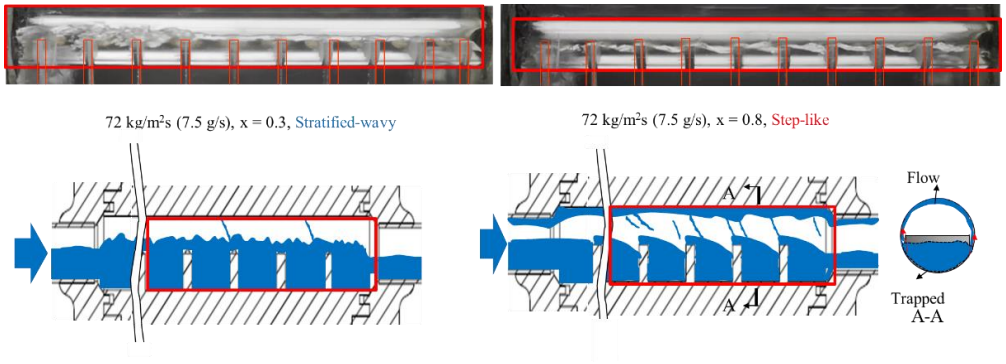

Figure 13: Flow patterns in the tube w/ header-like protrusion (horizontal flow with downward protrusions)

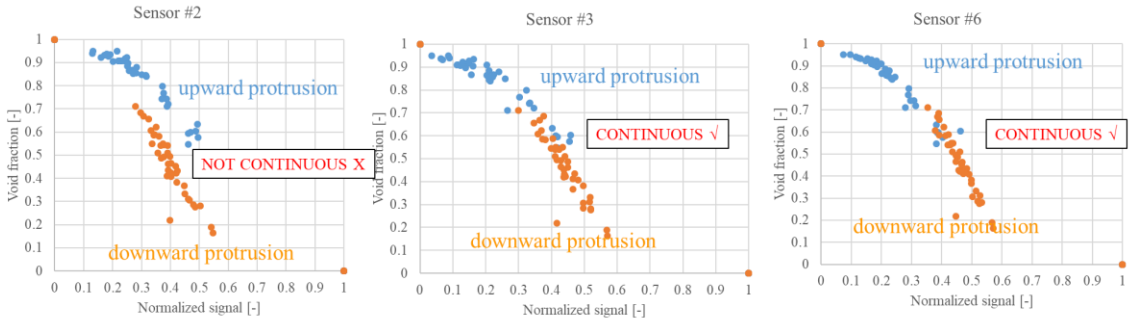

Figure 14: Relation between void fractions and normalized signals are continuous for sensors in both configurations. Some are not.

5. CONCLUSIONS

This paper presents the calibration procedures of the capacitive sensors for measuring void fraction in vertical and horizontal headers with R134a. Because the electric field within each sensor is not perfectly uniform, and all eleven sensors are not identical, calibrations are needed before measuring void fraction. The calibration is based on the following parameters: the average void fraction measurement with quick-closing valves, flow regime visualization, the pressure drop along the header, and capacitive signals analysis. After the calibration procedure, the sensors are capable of measuring void fractions in vertical headers. For the horizontal headers, further modifications or calibrations may be needed.

NOMENCLATURE

C	Capacitance signals	(pF)
D	Inner tube diameter	(mm)
G	Mass flux	(kg/m^{2}s)
L	Axial electrode length	(mm)
P	Absolute pressure	(kPa)
T	Temperature	(°C)
x	Vapor quality	(–)
α	Void fraction	(–)
Subscript		
vapor	Vapor phase	
liquid	Liquid phase	
measure	Measured values	
norm	Normalized	
sub	Subcool	
i	inlet	

REFERENCES

Abouelwafa, M. S. A., & Kendall, E. J. M. (1980). The use of capacitance sensors for phase percentage determination in multiphase pipelines. *IEEE Transactions on Instrumentation and measurement, 29*(1), 24-27.

Canière, H., T'Joen, C., Willockx, A., De Paepe, M., Christians, M., Van Rooyen, E., . . . Meyer, J. (2007). Horizontal two-phase flow characterization for small diameter tubes with a capacitance sensor. *Measurement Science and Technology, 18*(9), 2898.

Chen, I. Y., Tseng, C.-Y., & Wang, C.-C. (2010). Two-phase Flow Pressure Change across Sudden Contraction and Expansion in Small Channels.

Da Silva, M., Thiele, S., Abdulkareem, L., Azzopardi, B., & Hampel, U. (2010). High-resolution gas–oil two-phase flow visualization with a capacitance wire-mesh sensor. *Flow Measurement and Instrumentation, 21*(3), 191-197.

dos Reis, E., & Goldstein, L. (2005). A procedure for correcting for the effect of fluid flow temperature variation on the response of capacitive void fraction meters. *Flow Measurement and Instrumentation, 16*(4), 267-274.

Drahoš, J. í., & Čermák, J. (1989). Diagnostics of gas—liquid flow patterns in chemical engineering systems. *Chemical Engineering and Processing: Process Intensification, 26*(2), 147-164.

Friedel, L. (1978). Pressure-drop during gas-vapor-liquid flow in pipes. *Chemie Ingenieur Technik, 50*(3), 167-180.

Isbin, H. S., Sher, N. C., & Eddy, K. C. (1957). Void fractions in two-phase steam-water flow. *AIChE Journal, 3*(1), 136-142. doi:10.1002/aic.690030122

Qian, H., & Hrnjak, P. (2019). Void Fraction Measurement and Flow Regimes Visualization of R134a in Horizontal and Vertical ID 7 mm Circular Tubes. *International journal of refrigeration*. doi:https://doi.org/10.1016/j.ijrefrig.2019.04.018

Qian, H., & Hrnjak, P. (2020). Mass measurement based calibration of a capacitive sensor to measure void fraction for R134a in smooth tubes. *International journal of refrigeration, 110*, 168-177. doi:https://doi.org/10.1016/j.ijrefrig.2019.10.019

Qian, H., & Hrnjak, P. (2021). Characterization of R134a two-phase flow regimes in horizontal and vertical smooth tubes with capacitive sensors. *International journal of refrigeration*. doi:https://doi.org/10.1016/j.ijrefrig.2021.01.015

Tuo, H., & Hrnjak, P. (2013). Effect of the header pressure drop induced flow maldistribution on the microchannel evaporator performance. *International journal of refrigeration, 36*(8), 2176-2186. doi:https://doi.org/10.1016/j.ijrefrig.2013.06.002

Wojtan, L., Ursenbacher, T., & Thome, J. R. (2005). Measurement of dynamic void fractions in stratified types of flow. *Experimental Thermal and Fluid Science, 29*(3), 383-392. doi:https://doi.org/10.1016/j.expthermflusci.2004.05.017